

SafeNav: Safe Path Navigation using Landmark Based Localization in a GPS-denied Environment

Ganesh Sapkota, Sanjay Madria

Department of Computer Science, Missouri University of Science and Technology, Rolla, MO, USA

Email: {gsapkota, madrias}@mst.edu

Abstract—In battlefield environments, adversaries frequently disrupt GPS signals, requiring alternative localization and navigation methods. Traditional vision-based approaches like Simultaneous Localization and Mapping (SLAM) and Visual Odometry (VO) involve complex sensor fusion and high computational demand, whereas range-free methods like DV-HOP face accuracy and stability challenges in sparse, dynamic networks. This paper proposes LanBLoc-BMM, a navigation approach using landmark-based localization (LanBLoc) combined with a battlefield-specific motion model (BMM) and Extended Kalman Filter (EKF). Its performance is benchmarked against three state-of-the-art visual localization algorithms integrated with BMM and Bayesian filters, evaluated on synthetic and real-imitated trajectory datasets using metrics including Average Displacement Error (ADE), Final Displacement Error (FDE), and a newly introduced Average Weighted Risk Score (AWRS). LanBLoc-BMM (with EKF) demonstrates superior performance in ADE, FDE, and AWRS on real-imitated datasets. Additionally, two safe navigation methods, SafeNav-CHull and SafeNav-Centroid, are introduced by integrating LanBLoc-BMM(EKF) with a novel Risk-Aware RRT* (RAw-RRT*) algorithm for obstacle avoidance and risk exposure minimization. Simulation results in battlefield scenarios indicate SafeNav-Centroid excels in accuracy, risk exposure, and trajectory efficiency, while SafeNav-CHull provides superior computational speed.

Index Terms—Landmark-based Non-GPS localization, Visual Localization, GPS-Denied Environment, Safe Navigation

I. INTRODUCTION

In military operations, Safe navigation demands a precise and reliable positioning system [1], path planning, and maneuver decision support systems under adversarial conditions. Thus, positioning algorithms are central to safe navigation, especially on a battlefield, where precise location, timing, and coordination are critical for moving troops and ground vehicles.

Challenges: GPS provides reliable location data; however, its dependency on satellite signals makes it vulnerable to jamming and spoofing in combat scenarios.

Several methodologies have been developed to address localization and navigation challenges for GPS-denied environments, including Simultaneous Localization and Mapping (SLAM) [4], Visual Odometry (VO) [5], and other non-GPS-based techniques like DV-Hop Localization [9]. Although SLAM and VO excel in GPS-denied pose estimation, their heavy computational demand for high-resolution 3-D processing and reliance on multi-sensor fusion [15] make them not feasible for rapid-response systems in battlefield settings where soldiers use resource-constrained and battery-powered

mobile devices.

To address these challenges, [3] proposed LanBLoc, a localization framework for non-GPS battlefield environments using stereo vision and landmark recognition with passive camera sensors. However, it does not address navigation and motion planning based on landmark localization, which is the focus of this work.

This research proposes solutions to efficiently guide Moving Entities (ME) along a *safe path* in a non-GPS environment using LanBLoc as a location measurement model, ensuring efficient and safe navigation from source to destination.

To achieve our objective, we first define ground motion planning and extend it to a **Battlefield Motion Model (BMM)** that captures the non-linear dynamics of battlefield terrains, including obstacles and hazards. We then propose **LanBLoc-BMM**, a navigation approach combining LanBLoc for location measurement, BMM for motion planning, and EKF [13] to handle unmodeled influences of battlefield terrain. The model assumes sufficient detectable landmarks for trilateration [3] throughout the maneuver from source to destination. Additionally, we propose two safety check algorithms, **SafeNav-CHull** and **SafeNav-Centroid**, to ensure safe state transitions and controlled maneuvering within path boundaries. Integrated with LanBLoc-BMM(EKF), they enable efficient navigation. To handle obstacles, we introduce **Risk-Aware RRT* (RAw-RRT*)**, a variant of RRT* with a novel risk-aware cost function.

We evaluate the performance of the proposed algorithms using standard metrics such as Average Displacement Error (ADE), Final Displacement Error (FDE), and Percent Error. Additionally, we introduce the novel Average Weighted Risk Score (AWRS) metric that measures the trajectory safety based on deviations from hazard boundaries. The performance contributions of our research work are:

1) The LanBLoc-BMM (EKF) algorithm is evaluated against three state-of-the-art localization algorithms integrated with EKF and PF. LanBLoc-BMM achieves the highest accuracy with ADE/FDE of 0.4972/0.4675, lowest AWRS of 0.3492, and minimal runtime of 3.98 *ms* on synthetic datasets. For real-imitated trajectory datasets, LanBLoc-BMM (EKF) attains an ADE/FDE of 0.2393/0.3095, the lowest AWRS of 0.1528, and the shortest runtime of 14.94 *ms*.

2) Comparing SafeNav-Centroid and SafeNav-CHull algorithms integrated with RAw-RRT*, SafeNav-Centroid demonstrates superior accuracy and safety, with an average per-

cent error improvement of 16.12% over SafeNav-CHull, and ADE/FDE of 1.11/0.99 m that are 1.67 times (ADE) and 3.30 times (FDE) better.

Overall, SafeNav-Centroid generates the shortest path with less exposure to hazard, while SafeNav-Chull provides comparable results with higher computational efficiency.

II. RELATED WORKS

Recent advances in GPS-free positioning, such as SLAM, VO, and deep learning-based methods, have enhanced autonomous navigation in GPS-denied environments. Vision-based localization uses images or video to estimate a robot's position. SLAM [4] simultaneously builds maps and estimates pose but requires multi-sensor fusion (e.g., cameras, lidar). VO [6] tracks motion by analyzing frame-to-frame changes. Deep learning approaches [7], especially CNNs, have shown high accuracy across diverse settings.

DV-hop algorithms [9], popular in wireless sensor networks for their simplicity and low-cost hardware, estimate node positions based on hop counts to anchors. However, they perform poorly in dynamic or non-uniform networks due to sensitivity to node mobility.

For filtering, EKF [13] handles nonlinear systems through linearization and is well-suited for localization in battlefield environments due to its efficiency and robustness. Particle Filters (PFs) [14], while better for non-Gaussian systems, require careful tuning of particle count and resampling, impacting performance and computational load.

III. SAFE PATH NAVIGATION FRAMEWORK

Our system is designed to guide ME through a safe path starting from its current position to the destination. In the context of battlefield navigation, a safe path refers to a field that avoids obstacles and possible hazards. A continuous function that maps a parameter s representing a sequence to a point in the navigable space, such that the path avoids hazards, and collisions with obstacles, and respects the constraints of the navigable space as defined in Eqn. 1.

$$\mathbf{p}(s) : [s_0, s_f] \rightarrow \mathbb{R}^n \quad (1)$$

where s is the parameter, representing sequence, with s_0 and s_f being the start and end sequence numbers, \mathbb{R}^n represents the n -dimensional navigable space, $\mathbf{p}(s)$ is the position in the navigable space. The path starts at the initial position p_0 and ends at the target position p_f , given by Eqn. 2.

$$\mathbf{p}(s_0) = p_0, \quad \mathbf{p}(s_f) = p_f \quad (2)$$

The Control Center (CoC) generates the safe path using the ME's current state and environmental obstacles or hazards. Fig. 1 shows an overview of our proposed navigation framework for GPS-denied battlefield environments. The ME uses BMM & EKF for motion planning, LanBloc & IMU for state measurement, and SafeNav-Chull or SafeNav-Centroid for heading and maneuvering decisions. The ME initially obtains the safe path as a series of path segments $(s_1, s_2 \dots s_n)$ each containing trajectory points $p_i =$

$\{(x_{i1}, y_{i1}), (x_{i2}, y_{i2}), \dots, (x_{im}, y_{im})\}$ from the CoC via secure communication. Each path segment $s_i = (p_1, p_2, \dots, p_m)$ uses safety check algorithms to compute control commands. The process begins with the initial State $(x_i, y_i, v_i, \theta_i)$ which includes the initial position coordinates (x_i, y_i) , speed (v_i) and heading angle (θ_i) of the moving entity. The ME runs the stereo vision and YOLOv11-based localization algorithm (*LanBLoc*) to obtain its initial position and assumes to establish communication with the CoC via a secure communication protocol. However, the architecture of node communication with a CoC is not covered in this research work.

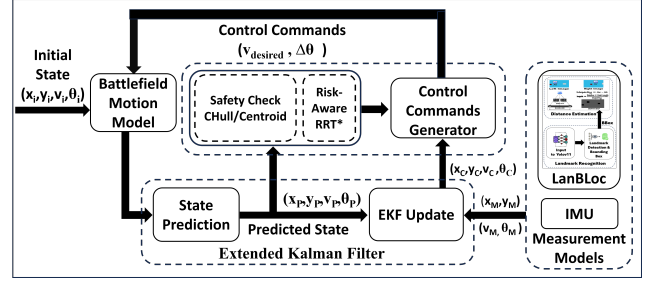


Fig. 1. An Overview of Safe Path Navigation Framework for GPS-denied Environment using Battlefield Motion Model (BMM), Extended Kalman Filter (EKF), and safety-checking algorithms (CHull and Centroid).

IV. PROPOSED METHODOLOGY

This section provides a detailed explanation of the proposed methodologies in the Safe Path Navigation Framework shown in Fig. 1.

A. Landmark-based localization (*LanBLoc*) of moving object

To address the challenges of deploying physical anchor nodes, recent research presents an alternative solution by recognizing the geographical landmarks as reference points using the YOLOv8-based landmark recognition model [3]. We improve this recognition model using YOLOv11s [8] to identify and precisely locate the reference landmarks. We utilized the pre-trained backbone of YOLOv11s and added a custom classifier head for landmark classification and bounding box coordinates. We utilized Generalized Intersection over Union (GIoU) for bounding box loss, Cross-entropy (CE) for landmark classification loss, and Binary cross-entropy (BCE) for the objectness score. The model was trained for 100 epochs with a batch size of 16 using *SGD* optimizer on the real-world landmark dataset (MSTLandmarkv1) [2] containing 34 landmark classes.

The landmark recognition model achieved high performance for training and validation. For training, it demonstrated a Box Loss Precision (Pr) of 0.938, Recall (R) of 0.963, and mAP @ 0.5 IoU of 0.968, with mAP @[0.5:0.95] IoU at 0.841. Validation results were similarly strong, with a Precision of 0.931, a Recall of 0.953, mAP @ 0.5 IoU of 0.964, and mAP @[0.5:0.95] IoU at 0.834 across all landmark classes.

The distances between the moving entity and the identified landmark anchors are calculated using an efficient stereo-matching technique [2] with high accuracy. Using the localized

landmark anchors and the calculated distances to the anchors, the LanBLoc algorithm computes the position of a moving object with an average RMSE of 0.0142m in the X-position and 0.039m in the Y-position.

B. Motion Planning of Moving Entity in the Battlefield

Motion planning in battlefield scenarios must account for both physical kinematics and tactical constraints. Our **Battlefield Motion Model (BMM)** captures key dynamics such as velocity, acceleration, deceleration, and maneuverability (max heading rate) to predict the next state from a given control input. Using update equations 3, 4, and 5, BMM models unit motion through position $\vec{p}_t = [x_t, y_t]$, velocity v_t , and heading θ_t , adjusted by desired speed v_{desired} , heading change $\Delta\theta$, acceleration a , deceleration d , and maneuverability m , updated at each time step Δt . Now, the motion model can then be expressed as:

1) Velocity Update:

$$v_{t+1} = \begin{cases} \min(v_t + a\Delta t, v_{\text{desired}}, v_{\text{max}}) & \text{if } v_{\text{desired}} > v_t \\ \max(v_t - d\Delta t, v_{\text{desired}}, 0) & \text{if } v_{\text{desired}} \leq v_t \end{cases} \quad (3)$$

where, v_{max} is the maximum speed of the unit.

2) Heading Update:

$$\theta_{t+1} = \theta_t + \text{clip}(\Delta\theta, -m\Delta t, m\Delta t) \quad (4)$$

3) Position Update:

$$\vec{p}_t = \vec{p}_{t-1} + v_{t-1} \cdot \Delta t \cdot \begin{bmatrix} \cos(\theta_{t-1}) \\ \sin(\theta_{t-1}) \end{bmatrix} \quad (5)$$

In this model, the next velocity v_{t+1} is computed from the current velocity v_t , constrained by acceleration, deceleration, and speed limits. Heading θ_{t+1} is adjusted by $\Delta\theta$ within maneuverability bounds, and the new position \vec{p}_{t+1} is calculated using the updated velocity and heading, assuming linear motion with instantaneous changes.

However, real battlefield dynamics are influenced by unpredictable factors like terrain, obstacles, and environmental changes. To reflect this, the motion model incorporates process noise in position, velocity, acceleration, and heading represented by terrain effects (τ) and noise terms $\epsilon_{x,t}, \epsilon_{y,t}, \epsilon_{v_x,t}, \epsilon_{v_y,t}, \epsilon_{a_x,t}, \epsilon_{a_y,t}, \epsilon_{\theta,t}$. The updated model is defined in Eqns. 6 and 7.

$$v_{t+1} = f(v_t, a_t, \epsilon_{v,t}, \epsilon_{a,t}), \quad \theta_{t+1} = \theta_t + \Delta\theta + \epsilon_{\theta,t} \quad (6)$$

where $\Delta\theta = \arctan(\Delta x / \Delta y)$ rate of heading change, and f is a function that computes the next velocity based on the current velocity, acceleration, and terrain. Next, the position of ME is estimated according to Eqn. 7

$$\begin{aligned} x_{t+1} &= x_t + v_{t+1} \cdot \Delta t \cdot \cos(\theta_{t+1}) + \epsilon_{x,t} \\ y_{t+1} &= y_t + v_{t+1} \cdot \Delta t \cdot \sin(\theta_{t+1}) + \epsilon_{y,t} \end{aligned} \quad (7)$$

Terrain effect τ significantly impacts position prediction accuracy. Accurately estimating τ improves navigation in complex

terrains. The total travel time from point P1 (x_1, y_1) to P2 (x_2, y_2), accounting for τ , is given by Eqn. 8.

$$t_\tau = \frac{\|P_1 - P_2\|}{v_c} + \lambda \quad (8)$$

where $\lambda = \tau / v_c$ represents the time delay caused by terrain effect τ , initially estimated using prior knowledge. As terrain and velocity vary, τ may change during navigation. The predicted position p_{t+1} accounting for τ is given in Eqn. 9.

$$p_{t+1} = p_t + v_{t+1} \cdot t_\tau \cdot \begin{bmatrix} \cos(\theta_{t+1}) \\ \sin(\theta_{t+1}) \end{bmatrix} + \begin{bmatrix} \epsilon_{x,t} \\ \epsilon_{y,t} \end{bmatrix} \quad (9)$$

where p_t is the current position of the ME.

The Eqn. 9 captures the essential dynamics of the motion model for any moving entities on a battlefield, considering their physical capabilities and the control inputs for navigation.

C. Trajectory Estimation using BMM and EKF

The Extended Kalman Filter (EKF) for the non-linear battlefield scenario linearizes the current mean and covariance, allowing it to approximate the state of a nonlinear system, and thus is an effective filtering algorithm due to its low computational complexity and high estimation accuracy. We adapted an EKF [13] by integrating the BMM defined in Eqns. 6 and 7 in its prediction step to predict the future state of a moving entity.

The state transition function X_{k+1} and the measurement function Z_{k+1} are represented in Eqn. 10. The predicted state estimate \hat{x}_{k+1} and predicted covariance estimate P_{k+1} are given by Eqn. 11. The measurement residual \tilde{y}_{k+1} and residual covariance S_{k+1} are calculated using Eqn. 12.

$$X_{k+1} = f(X_k, U_k) + W_k, \quad Z_{k+1} = h(X_{k+1}) + V_{k+1} \quad (10)$$

$$\hat{x}_{k+1} = f(\hat{x}_k, U_k) + w_k, \quad P_{k+1} = F_k \cdot P_k \cdot F_k^T + Q_k \quad (11)$$

$$\tilde{y}_{k+1} = z_k - h(\hat{x}_{k+1}), \quad S_{k+1} = H_{k+1} \cdot P_{k+1} \cdot H_{k+1}^T + R_{k+1} \quad (12)$$

where, $f(\cdot)$ is the nonlinear state transition function, U_k is the control input, and X_k is the previous state. $h(\cdot)$ represents the LanBLoc measurement function. W_k and V_{k+1} are process and measurement noise, assumed to be normally distributed with covariances Q_k and R_{k+1} , respectively. F_k is the Jacobian of $f(\cdot)$ with respect to X , evaluated at \hat{x}_{k+1} . z_{k+1} is the observed position at time $k+1$.

The Kalman Gain is a fundamental component of the Kalman Filter that determines the degree to which the new measurement will be incorporated into the state estimate.

So, the Kalman Gain K_{k+1} is computed using the predicted covariance estimate P_{k+1} , the transpose of the observation model H_{k+1}^T , and the inverse of the residual covariance S_{k+1}^{-1} in equation 13 below.

$$K_{k+1} = P_{k+1} \cdot H_{k+1}^T \cdot S_{k+1}^{-1} \quad (13)$$

Algorithm 1 Safety Check using Convex Hull Method

Require: current position p_t , v_t , θ_t , a_t , $\epsilon_{v,t}$, $\epsilon_{\theta,t}$, t_τ , list of path segments $S = \{s_i..s_n\}$

Ensure: Estimated Position p_{t+1} and Control Input U

```
1: procedure CONVEXHULL( $p_t, v_t, \theta_t, a_t, \epsilon_{v,t}, \epsilon_{\theta,t}, t_\tau$ )
2:   Update  $v_{t+1} \leftarrow f(v_t, a_t, \epsilon_{v,t})$ 
3:   Update  $\theta_{t+1} \leftarrow \theta_t + \Delta\theta + \epsilon_{\theta,t}$ 
4:   Estimate:  $p_{t+1} \leftarrow p_t + (v_{t+1} \cdot t_\tau \cdot \cos(\theta_{t+1}), v_{t+1} \cdot t_\tau \cdot \sin(\theta_{t+1}))$ 
For Each:  $segment\ s_i$  in  $S$ 
5:    $current\_hull \leftarrow ConvexHull(segment)$ 
6:    $next\_segment\_index \leftarrow \text{index of next segment}$ 
7:   if  $next\_segment\_index$  exists then
8:      $next\_hull \leftarrow ConvexHull(next\_segment)$ 
9:   end if
10:  if PointInHull( $predicted\_position, current\_hull$ ) or ( $next\_hull$  is not None) then
11:    return  $p_{t+1}$ 
12:  else
13:    Compute:  $ControlInput(current\_hull, next\_hull)$ 
14:    break
15:  end if
16:  return  $p_{t+1}$  and  $U(v_i, \theta_i)$ 
17: end procedure
```

Finally, the state estimate \hat{x}_{k+1} and covariance estimate P_{k+1} are updated in Eqn. 14.

$$\hat{x}_{k+1} = \hat{x}_k + K_{k+1} \cdot \tilde{y}_{k+1}, \quad P_{k+1} = (I - K_{k+1} \cdot H_{k+1}) \cdot P_{k+1} \quad (14)$$

Where I is the identity matrix.

D. Safety Check and Controlled Maneuver

1) *Convex Hull Method:* The convex hull method offers a geometrically robust and computationally efficient way to define safe navigation boundaries. In our approach, it verifies whether the predicted position lies within a safe zone while steering toward a look-ahead point. The path is divided into sequential segments, each represented as $S = (x_1, y_1), \dots, (x_n, y_n)$, and their convex hulls are computed using Chan's algorithm [10]. The predicted state is then checked using a point-in-polygon test [11].

At each trial's start, the node's initial position (x_i, y_i) is obtained via LanBLoc, while velocity (v_i) and heading (θ_i) are measured using an IMU sensor simulator. These inputs feed into the EKF module, which predicts the next state $(x_P, y_P, v_P, \theta_P)$ as detailed in Section IV-B. The node then checks if the predicted position lies within the convex hull of the current or next segment. If so, it proceeds with default control commands; otherwise, it recalculates them or steps back if outside adjacent hulls. Trajectory prediction and safety checks are detailed in Sections IV-C and Algorithm 1, respectively.

2) *Centroid Method:* The Centroid Method relies on the centroids of sub-segments within a safe path to compute the control commands. In this approach, the current path segment is divided into smaller sub-segments, and the centroids of these sub-segments are calculated. The algorithm determines the closest centroid to the entity's current position (updated by EKF) and computes the control input $U(v_i, \theta_i)$ required to reach the centroid. Using these control commands, it predicts the next position of the entity, which is mentioned in detail in the Algorithm 2. This algorithm attracts the moving entity toward the centroid of the path segment to minimize the drift from the central trajectory.

Algorithm 2 Safety Check using Centroid Method

Require: current position p_t , v_t , θ_t , a_t , $\epsilon_{v,t}$, $\epsilon_{\theta,t}$, t_τ , list of path segments $S = \{s_i..s_n\}$

Ensure: Estimated Position p_{t+1} and Control Input U

```
1: procedure ESTIMATENEXTPOSITION( $p_t, v_t, \theta_t, a_t, \epsilon_{v,t}, \epsilon_{\theta,t}, t_\tau, s_i$ )
2:   calculate centroids  $C \leftarrow \{c_j..c_n\}$ 
3:   Select  $c_j \leftarrow \arg \min_{c_j \in C} \|c - p_c\|$ 
4:   Compute  $U(v, \theta_i)$ :  $v_i = v_t, \Delta\theta = \arctan(\Delta x / \Delta y)$ 
5:   Update  $v_{t+1} = f(v_t, a_t, \epsilon_{v,t})$ ,  $\theta_{t+1} \leftarrow \theta_t + \Delta\theta + \epsilon_{\theta,t}$ 
6:    $p_{t+1} \leftarrow p_t + (v_{t+1} \cdot t_\tau \cdot \cos(\theta_{t+1}), v_{t+1} \cdot t_\tau \cdot \sin(\theta_{t+1}))$ 
7:   return  $p_{t+1}$  and  $U(v_i, \theta_i)$ 
8: end procedure
```

E. Risk Minimization and Obstacle Avoidance using Risk-Aware RRT*

1) *Rapidly Exploring Random Tree-Star (RRT*):* RRT* [12] finds the shortest obstacle-free path using:

$$Cost(p) = \sum_{i=1}^{n-1} \|\mathbf{x}_i - \mathbf{x}_{i+1}\| \quad (15)$$

2) *Risk-Aware RRT* (RAw-RRT*):* We extend RRT* to include hazard awareness via a modified cost:

$$C_{total} = \alpha \cdot C_{length} + \beta \cdot C_{risk} \quad (16)$$

Here, C_{length} is the total Euclidean path length, and C_{risk} sums the Weighted Risk Scores (WRS) across trajectory points. Parameters α and β balance between path length and risk exposure. This version is used to re-generate safe paths during CHull and Centroid-based motion.

3) *Edge-Wise WRS Calculation:* Deviation from the central path is calculated using Eqn. 17 and WRS is computed based on zone-specific deviation using Eqn. 18.

$$d_i = \|\mathbf{p}_i - \mathbf{c}_i\| \quad (17)$$

$$WRS(\mathbf{p}_i) = \begin{cases} |d_i| \times \left(\frac{|d_i|}{w_j}\right) & \text{if } a_j \leq |d_i| < b_j \\ d_{max} \times \left(\frac{d_{max}}{w_{max}}\right) & \text{if } |d_i| \geq d_{max} \end{cases} \quad (18)$$

where w_j is the zone weight and w_{max} applies for large deviations exceeding d_{max} .

4) *Total Trajectory Cost*: For a trajectory with points $\{\mathbf{p}_i, \dots, \mathbf{p}_n\}$, the total risk-aware cost is given by Eqn. 19.

$$C_{\text{total}} = \alpha \sum_{i=1}^{n-1} \|\mathbf{p}_i - \mathbf{p}_{i+1}\| + \beta \sum_{i=1}^n \text{WRS}(\mathbf{p}_i) \quad (19)$$

*F. Safe Path Navigation using SafeNav-Chull and SafeNav-Centroid and RAw-RRT**

The complete steps to guide the object from a start to the end position along a pre-defined safe path are presented in Algorithm 3. This algorithm includes the navigation steps for both SafeNav-Chull and SafeNav-Centroid when integrated with RAw-RRT*.

Algorithm 3 Safe Path Navigation

Require: Initial position $p_t, v_t, \theta_t, a_t, \epsilon_{v,t}, \epsilon_{\theta,t}, t_\tau$, control input U_i , path segments $S = \{s_i..s_n\}$

Ensure: Predicted and Actual trajectory list

- 1: Select the Method $\in \{\text{Algorithm 1, Algorithm 2}\}$
 - 2: **for** $\text{path_segment } \{s_i\} \in S$ **do**
 - 3: $\text{nextPosition} = \text{EstimateNextPosition}(p_t, v_t, \theta_t, a_t, \epsilon_{v,t}, \epsilon_{\theta,t}, t_\tau, s_i)$
 - 4: $U_i = (v_i, \theta_i)$
 - 5: Check for Obstacles:
 - 6: **if** $\text{ObstacleDetected}(p_t, s_i, O)$ **then**
 - 7: Use **equation 19** to find alternative path to nextPosition that minimize cost.
 - 8: **end if**
 - 9: Move the object to the nextPosition p_{t+1} .
 - 10: Measure current state using $\text{LanBloc}() + \text{IMU} + \text{EKF}$
 - 11: Append predicted state to *predicted* and measured state to *measured*
 - 12: Update U_i based on the current and next states
 - 13: **end for**
 - 14: **return** *predicted* and *measured*
-

V. EXPERIMENTS AND RESULTS

To test the validity of our proposed navigation algorithms, experiments were performed on an Alienware Aurora R12 System with an 11th Gen Intel Core i7 CPU, 32 GiB of Memory, and an Nvidia GeForce RTX 3070 GPU using Python 3.11 on PyCharm CE 2024 IDE. The landmark recognition model was trained using Python 3.10.12 and torch 2.5.1+cu121, utilizing an NVIDIA A100-SXM4 GPU with 40GB of memory.

A. Datasets

1) *Landmark and Stereo Vision Dataset*: We used the publicly available MSTlandmarkv1 dataset to train the landmark recognition model and MSTlandmarkStereov1 for distance estimation from [2].

2) Trajectory Dataset and Safe Path:

i) Synthetic Trajectory Dataset: Trajectories were generated using initial parameters for acceleration and heading angle over time, calculated for each timestep i as:

$$a(t_i) = 3 \sin\left(\frac{4\pi t_i}{T}\right), \quad \theta(t_i) = \frac{\pi}{2} \sin\left(\frac{2\pi t_i}{T}\right)$$

With N timesteps and a timestep size of $dt = 0.05s$, the total duration was $T = N \cdot dt$. Each trajectory point was represented by seven state variables: $p_x, s_x, a_x, p_y, s_y, a_y, \theta$, denoting positions, speeds, accelerations along the x and y axes, and heading direction.

ii) Real-Imitated Trajectory Dataset: We generated real-imitated trajectories and safe path datasets to validate our navigation framework. A virtual battlefield region of a 200×200 grid was created, mapping landmarks from the MSTlandmark-Stereov1 datasets. We randomly placed 25 obstacles and 25 hazard components within this grid to simulate battlefield conditions. Clusters containing at least three landmarks within detectable range were selected as a trilateration set for LanBloc localization. Path clusters, comprising sequences of these landmark clusters, were used to generate ground truth trajectories by navigating through cluster centroids.

iii) Safe Path Buffer and Risk Zone: A safe buffer is a bounded region around the ground truth trajectory, divided into four equal-width zones with risk weights $w_1 = 2$, $w_2 = 4$, $w_3 = 6$, and $w_4 = 8$. The Weighted Risk Score (WRS), calculated using Eqn. 18, increases with distance from the central trajectory, quantifying navigation risk based on deviation.

B. Evaluation Metrics

We used standard metrics such as ADE, FDE, and Percent Error to evaluate trajectory accuracy, along with a novel AWRS to assess risk exposure. Each safe path was simulated over 1000 trials and averaged.

The AWRS is defined as the mean of the individual Weighted Risk Scores across all trajectory points: $\text{AWRS} = \frac{1}{N} \sum_{i=1}^N \text{WRS}_i$, Where N is the total number of trajectory points and WRS_i is the weighted risk score for the i^{th} point calculated using Eqn. 18. ADE is the mean L2 distance between the estimated and ground truth trajectory: $\text{ADE} = \frac{1}{N} \sum_{t=t_0}^{t_f} \|\hat{Y}_t - Y_t\|$. FDE is the L2 distance between the estimated and ground truth trajectory at the final time step: $\text{FDE} = \|\hat{Y}_{t_f} - Y_{t_f}\|$. Percent Error is given by $\frac{|\text{Est. Length} - \text{True Length}|}{\text{True Length}} \times 100\%$.

C. Simulation and Experimental Results Discussion

Baselines:

We evaluated the proposed LanBLoc-BMM against state-of-the-art methods—DeepLoc-GPS, DeepLoc-EKF-GPS [6], and Multi-Sensor Fusion [15]—using both synthetic and real-imitated datasets. Performance with EKF and PF on synthetic and real datasets is summarized in Tables I and II, respectively. Table I highlights the best overall performance of LanBLoc(EKF), with the lowest ADE, FDE, AWRS, and runtime,

while DeepLoc-GPS-EKF (*EKF*) is a close contender, performing well in all metrics, particularly in FDE and AWRS. DeepLoc-GPS (*EKF*) also performs well, especially in ADE and FDE; however, it lags in runtime. Sensor Fusion (EKF), while having the highest ADE, shows competitive FDE but is less efficient in computation. From Table II, it is evi-

TABLE I
PERFORMANCE ACROSS ALGORITHMS ON SYNTHETIC TRAJECTORY DATA

Algorithm	Filter	ADE/FDE (m)	AWRS	Time(ms)
DeepLocGPS	EKF	0.6069 / 0.5495	0.3926	5.02
	PF	1.1335 / 1.7614	2.1414	9815
DeepLocGPSEKF	EKF	0.5621 / 0.4818	0.3590	4.57
	PF	1.4864 / 1.5709	1.7823	10054
Sensor Fusion	EKF	1.3546 / 0.5714	0.3513	4.90
	PF	1.9155 / 3.1229	2.9387	10103
LanBLoc-BMM	EKF	0.4972 / 0.4675	0.3492	3.98
	PF	0.9471 / 0.8177	1.2612	9551

dent that LanBLoc-BMM (EKF) is best regarding accuracy, weighted risk score, and runtime for real trajectory datasets. It consistently offers the most accurate results with reasonable computation times and minimal risk exposure, making it the preferred choice for accurate and efficient localization across different path types. DeepLocGPS(EKF) provides its best accuracy with an ADE/FDE of 0.3041/0.3103, AWRS of 0.2009, and a reasonable runtime of 20.58 ms. DeepLocGPSEKF shows the best accuracy with an ADE/FDE of 0.2869/0.2969, AWRS of 0.1906, and a runtime of 18.94 ms. Sensor Fusion(EKF) provides a balance of accuracy (ADE/FDE of 0.2998/0.3115), AWRS of 0.1749, and an acceptable runtime of 22.31 ms. The proposed LanBLoc-BMM (EKF) based navigation again stands out with the best accuracy (ADE/FDE of 0.2393/0.3095), AWRS of 0.1528, and a low runtime of 14.94 ms.

TABLE II
AVERAGE ADE, FDE, WRS, AND RUNTIME(MS) VALUES FOR REAL-IMITATED TRAJECTORY FROM THREE PATH TYPES [P1, P2, P3] ACROSS DIFFERENT ALGORITHMS AND FILTER SCENARIOS.

Algorithm	Filter	ADE / FDE(m)	AWRS	Time(ms)
DeepLocGPS	EKF	0.3041 / 0.3103	0.2009	20.58
	PF	1.6928 / 2.8891	4.3586	192621
DeepLocGPSEKF	EKF	0.2869 / 0.2969	0.1906	18.94
	PF	2.0672 / 7.1665	3.6346	197250
Sensor Fusion	EKF	0.2998 / 0.3115	0.1749	22.31
	PF	1.6831 / 4.2886	5.4116	198790
LanBLoc-BMM	EKF	0.2393 / 0.3095	0.1528	14.94
	PF	1.5162 / 1.4024	3.1623	185502

D. Safe Path Navigation using SafeNavChull and SafeNav-Centroid with RiskAware RRT*

We developed two navigation methods called SafeNav-Chull and SafeNav-Centroid by integrating LanBLoc-BMM(*EKF*) with safety checks based on Algorithms 1 and 2, respectively. Both methods incorporate the proposed RAW-RRT* for obstacle avoidance and risk minimization within the safe path. To evaluate their effectiveness, we conducted trials on three path types formed by sequences of cluster members

with different origins and a common destination. The resulting trajectories are shown in Fig. 2 and Fig. 3. Each path type was simulated over 1000 trials, and performance was evaluated using ADE, FDE, AWRS, percent error, and runtime metrics.

1) *Average Percent Error in Trajectory Lengths*: Table III shows the trajectory length error for path types *P1*, *P2*, and *P3*. SafeNav-CHull shows an average error of 6.51%, while SafeNav-Centroid improves this to 5.46%. Notably, *P2* has the highest error across all methods, likely due to increased drift caused by noise in velocity and heading factors sensitive to terrain complexity and frequent directional changes.

TABLE III
PATH LENGTH ERROR OF ESTIMATED TRAJECTORIES FOR EACH PATH TYPE

Approaches	Path Type: Avg. % Error			Overall Avg.
	P1	P2	P3	
SafeNav-CHull	5.755	7.42	6.35	6.51
SafeNav-Centroid	5.32	5.60	5.47	5.46

2) *Displacement Errors and Weighted Risk Scores*: Table IV compares ADE, FDE, and AWRS across three path types (*P1*–*P3*). SafeNav-Centroid consistently outperforms SafeNav-CHull, with 1.67 times lower ADE and 3.30 times lower FDE, indicating higher accuracy and precision. Its lower final displacement errors suggest better alignment with the intended destination.

TABLE IV
COMPARISON OF ADE/FDE, AWRS, AND TIME FOR SAFENAV-CHULL AND SAFENAV-CENTROID

Approaches	Path Type	ADE / FDE	AWRS	Time(ms)
SafeNav-CHull	P1	2.73 / 3.16	1.31	14.93
	P2	2.72 / 3.08	1.11	14.84
	P3	3.46 / 3.57	1.71	15.98
	Average	2.97 / 3.27	1.38	15.25
	P1	1.06 / 0.87	1.01	16.74
SafeNav-Centroid	P2	1.13 / 1.03	1.01	16.94
	P3	1.15 / 1.06	1.01	16.97
	Average	1.11 / 0.99	1.01	16.88

VI. CONCLUSION AND FUTURE WORKS

In this paper, we present LanBLoc-BMM(EKF), an efficient navigation approach combining LanBLoc-based location measurement, BMM motion planning, and EKF integration. Building on this, we propose two safe path navigation algorithms, SafeNav-Chull and SafeNav-Centroid, which guide mobile troops along obstacle-free paths in GPS-denied battlefield environments. These algorithms combine geometric properties of the path segments (Convex Hull, Centroid) with a novel Risk-Aware RRT* and LanBLoc-BMM(EKF), achieving outstanding performance on localization and trajectory estimation.

Experimental results validate their effectiveness, showcasing their potential to significantly enhance the safety and operational efficacy of military forces in challenging and hostile environments. These approaches address the critical vulnerability of GPS reliance, ensuring troops can maneuver safely and

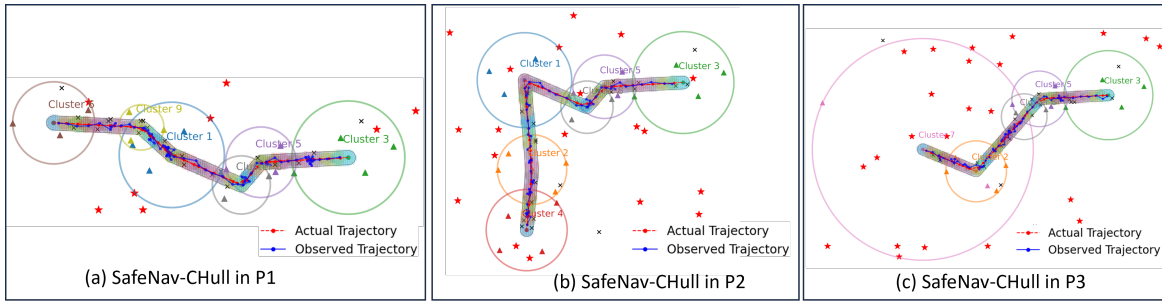


Fig. 2. Safe path navigation using SafeNav-Chull and RAW-RRT across three path types ($P1-P3$) from different clusters to the common destination (cluster 3). Colored segments represent convex hulls; red and blue lines indicate actual and observed trajectories.

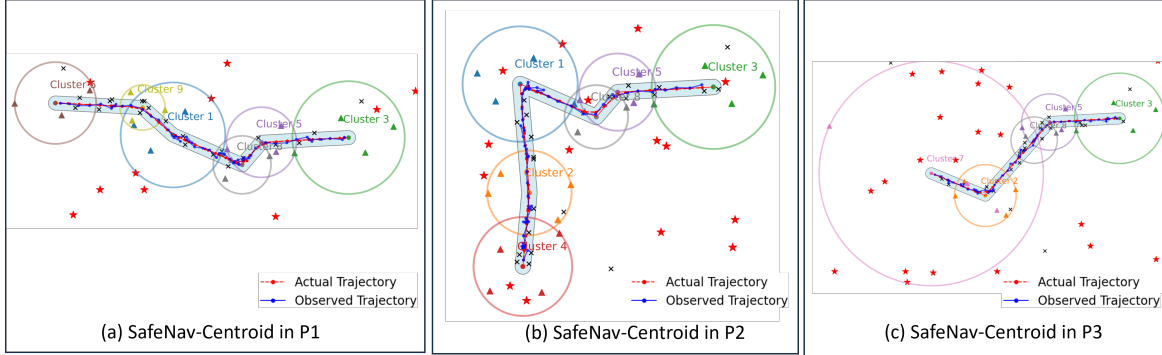


Fig. 3. Safe path navigation using SafeNav-Centroid and RAW-RRT across three path types ($P1-P3$) from different clusters to a common destination (cluster 3). Red and blue lines represent actual and observed trajectories, respectively.

efficiently in contested and hazardous areas. Future work will target reduced computational demand, enhanced adaptability to dynamic threats, and alternative localization methods for landmark-sparse settings.

ACKNOWLEDGEMENT

This research was funded by the Army Research Laboratory under Cooperative Agreement Number W911NF2120261. The opinions in this paper are the authors' and do not reflect the Army Research Laboratory's or the U.S. Government's official stance. The U.S. Government can legally reproduce and share this content for governmental use, despite any copyright claims.

REFERENCES

- [1] Shentu, S., Gong, Z., Liu, XJ. et al. Hybrid Navigation System Based Autonomous Positioning and Path Planning for Mobile Robots. Chin. J. Mech. Eng. 35, 109 (2022).
- [2] G. Sapkota and S. Madria, "Landmark Stereo Dataset for Landmark Recognition and Moving Node Localization in a Non-GPS Battlefield Environment," 2023 IEEE Applied Imagery Pattern Recognition Workshop (AIPR), St. Louis, MO, USA, 2023, pp. 1-11.
- [3] G. Sapkota and S. Madria, "Landmark-based Localization using Stereo Vision and Deep Learning in GPS-Denied Battlefield Environment," IEEE 25th International Symposium on a World of Wireless, Mobile and Multimedia Networks (WoWMoM), Perth, Australia, 2024, pp. 209-215.
- [4] C. Campos, R. Elvira, J. J. G. Rodríguez, J. M. M. Montiel and J. D. Tardós, "ORB-SLAM3: An Accurate Open-Source Library for Visual, Visual-Inertial, and Multimap SLAM," in IEEE Transactions on Robotics, vol. 37, no. 6, pp. 1874-1890, Dec. 2021.

- [5] A. Neyestani, F. Picariello, A. Basiri, P. Daponte and L. D. Vito, "Survey and Research Challenges in Monocular Visual Odometry," 2023 IEEE International Workshop on Metrology for Living Environment (Metro-LivEnv), Milano, Italy, 2023, pp. 107-112.
- [6] N. Engel, S. Hoermann, M. Horn, V. Belagiannis and K. Dietmayer, "DeepLocalization: Landmark-based Self-Localization with Deep Neural Networks," 2019 IEEE Intelligent Transportation Systems Conference (ITSC), Auckland, New Zealand, 2019, pp. 926-933.
- [7] J. Zhu, Y. Jia, W. Shen and X. Qian, "A Pose Estimation Method in Dynamic Scene with Yolov5, Mask R-CNN and ORB-SLAM2," 2022 7th International Conference on Signal and Image Processing (ICSIP), Suzhou, China, 2022, pp. 665-670.
- [8] Glenn Jocher, Ayush Chaurasia, and Jing Qiu, Ultralytics YOLO version 8.0.0, Jan. 2023. url: <https://github.com/ultralytics/ultralytics>.
- [9] Zhao, Qing et al. "An Improvement of DV-Hop Localization Algorithm Based on Cyclotomic Method in Wireless Sensor Networks." Applied Sciences (2023): n. pag.
- [10] Chan, Timothy M. "Optimal output-sensitive convex hull algorithms in two and three dimensions." Discrete and Computational Geometry 16.4 (1996): 361-368.
- [11] Galetzka, Michael and Patrick O. Glauner. "A Simple and Correct Even-Odd Algorithm for the Point-in-Polygon Problem for Complex Polygons." VISIGRAPP (2012).
- [12] Karaman, S., & Frazzoli, E. (2011). Sampling-based algorithms for optimal motion planning. The international journal of robotics research, 30(7), 846-894.
- [13] D. Feng, C. Wang, C. He, Y. Zhuang and X. -G. Xia, "Kalman-Filter-Based Integration of IMU and UWB for High-Accuracy Indoor Positioning and Navigation," in IEEE Internet of Things Journal, vol. 7, no. 4, pp. 3133-3146, April 2020.
- [14] Malviya, V., Kala, R. Trajectory prediction and tracking using a multi-behavior social particle filter. Appl Intell 52, 7158-7200 (2022).
- [15] K. Zhu, C. Deng, F. Zhang, H. Kang, Z. Wen and G. Guo, "A Multi-Source Fusion Navigation System to Overcome GPS Interruption of Unmanned Ground Vehicles," in IEEE Access, vol. 11, pp. 61070-61081, 2023.